



Nanosecond-pulsed laser welding of metallic glass

Jin Feng Li^{a,b}, Yong Hao Sun^{a,b,c,*}, Da Wei Ding^{a,b,c}, Wei Hua Wang^{a,b,c}, Hai Yang Bai^{a,b,c,*}

^a Institute of Physics, Chinese Academy of Sciences, Beijing, 100190, China

^b Center of Materials Science and Optoelectronics Engineering, University of Chinese Academy of Sciences, Beijing, 100049, China

^c Songshan Lake Materials Laboratory, Dongguan, Guangdong, 523808, China



ARTICLE INFO

Keywords:

Metallic glass
Laser welding
Welding parameter map
Thickness
Strength

ABSTRACT

This study explores nanosecond-pulsed (*ns*-pulsed) laser welding on the metallic glass (MG) ribbons of four compositions: Fe₇₈Si₉B₁₃, Zr₆₅Cu₁₅Ni₁₀Al₁₀, La₅₅Ni₂₀Al₂₅ and Ce₆₅Al₁₀Cu₂₀Co₅. All MGs can be welded in the air by the *ns*-pulsed laser, and the crystallization of the welding joints can be avoided by proper control of the laser parameters. By varying the travel speed, pulse duration and repetition frequency, the critical crystallization time of MG can be quickly detected in a high-throughput way by *ns*-pulsed laser welding. At the optimal processing conditions, 70–90% of the tensile strength of the parent melt-spun ribbon can be preserved in the welded MG ribbons. The mechanical strength is well linked to the profile of the welding joint, which suggests a simple method to evaluate the welding quality. A welding parameter map has been established based on the experiments, and it is concluded that the laser power-density per sample thickness and the interaction time are the key factors that control the crystallization and strength of the welding joints. The map is valid for a broad range of MG compositions of all sample thickness, and thus the optimal processing conditions may be extended to all MGs with equivalent glass-forming ability.

1. Introduction

Metallic glass (MG) welding remains a great challenge as it requires not only to join MG parts together but also to avoid crystallization and to maintain strength of the welding joints. Metallic liquids can easily form crystals when they are in the supercooled liquid region. Even with some best glass-forming compositions, the minimal time for crystallization is just several tens of milliseconds [1–5]. Crystallization is a serious problem as it induces embrittlement and weakens the overall strength. Over the last two decades, many joining techniques have been used to weld MGs, including friction [6–14], friction stir spot [15–21], spark [22], ultrasonic [23–25], explosion [26–28], electron-beam [29–36], magnetic [37] and laser welding [38–50]. Among lots of candidates, laser welding attracts great attention due to its high precision, fast speed, high energy-density and low cost [43,51]. Furthermore, the pulsed laser is better than the continuous wave laser because it shortens the interaction time at the high temperature, reducing the risk of crystallization. Using millisecond-pulsed (*ms*-pulsed) lasers, one-millimeter thick MG plates can be joined [38–50], but the simultaneous crystallization always remains problematic. The difficulty has to be overcome either by using limited good glass formers [41] or by placing a cooling apparatus underneath the specimen [44]. Furthermore, the *ms*-pulsed lasers used for welding above 1 mm plates, are not suitable to

thin ribbons because they often render excessive penetration. In comparison, *ns*-pulsed laser may be a better choice for MG ribbon welding because it has shorter pulse duration and smaller power-density.

Many welding parameters, e.g. the laser power, pulse duration and repetition frequency, travel speed of the laser head, can influence the quality of the welding joint, so finding the optimal control parameters for different materials is undoubtedly preferred. In addition, the welding profile reflects the quality of the welding joint, so an examination of the welding profile helps to amend the welding conditions. Besides, adjacent to the welded pool, the heat-affected zone (HAZ) is often the birthplace of crystallization, so specific care is required to make an accurate observation on the HAZs.

Nanosecond-pulsed lasers (*ns*-pulsed lasers) are enabled by using the Q-switching technique, where the population inversion can be quickly built up to a high level and rapidly deplete up when laser action terminates [52,53]. The *ns*-pulsed laser has been used to study how irradiation affects MGs but not paid much attention to its potential application on welding. In this work, we apply a ytterbium-doped optical-fiber *ns*-pulsed laser to lap- or butt- weld MG ribbons. Through *ns*-pulsed laser welding, both of the amorphicity and fracture strength are kept, proving that *ns*-pulsed laser can replace *ms*-pulsed laser for MG welding.

* Corresponding authors.

E-mail addresses: ysun58@iphy.ac.cn (Y.H. Sun), hybai@iphy.ac.cn (H.Y. Bai).

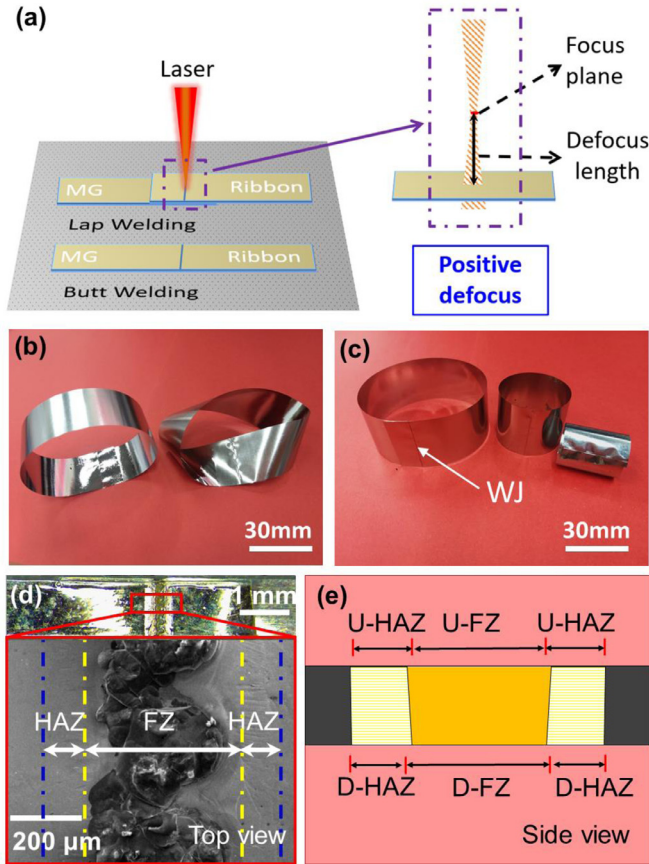


Fig. 1. The MG nanosecond-pulsed laser welding. (a) The schematic of the lap/butt-welding. (b) Ribbons are welded into a bracelet and a “Möbius band”. (c) Welded bracelets with different diameters (WJ: welding joint). (d) Top view of a welding joint examined by LDFM (top part) and SEM (bottom part). (FZ: fusion zone; HAZ: heat-affected zone). (e) Side view of a welding joint. (U: upside; D: downside).

2. Materials and methods

The $\text{Fe}_{78}\text{Si}_9\text{B}_{13}$, $\text{Zr}_{65}\text{Cu}_{15}\text{Ni}_{10}\text{Al}_{10}$, $\text{La}_{55}\text{Ni}_{20}\text{Al}_{25}$ and $\text{Ce}_{65}\text{Al}_{10}\text{Cu}_{20}\text{Co}_5$ MG compositions were selected. Master alloys were prepared by arc-melting the high purity elements, including Ce (99.5%), Al (99.99%), Cu (99.9%), Co (99.99%), Zr (99.9%), Ni (99.9%) and La (99.5%), under a Ti-gettered argon atmosphere. Ribbons with a thickness of 30–60 μm were prepared by melt spinning the molten liquid at 1100 K onto a copper wheel at a rotation speed of 40 r/min in an argon atmosphere. The $\text{Fe}_{78}\text{Si}_9\text{B}_{13}$ ribbon, 25 μm thick and 30 mm wide, was supplied by the Advanced Technology and Materials Co., Ltd., of Central Iron and Steel Research Institute. A ns-pulsed optical-fiber laser (Shenzhen JPT OPTO Electronics CO., LTD.) was used for welding with a laser wavelength of 1064 nm, an output power of 20 W, and a focused beam diameter of 50 μm .

The lap- and butt- welding were studied. For lap welding, one end of the ribbon was placed on top of the end of another ribbon; for butt welding, welding was done on one ribbon [Fig. 1(a)]. A 1 mm-thick quartz-glass slide with a transmittance of 0.83 was placed on top of the ribbons in welding. Positive defocus condition, where the focus of the laser was set above the sample position, was maintained throughout the experiments. The pulse duration (τ), travel speed (v) and repetition frequency (f) were set at 4 or 6 ns, 160 or 162 mm/s and 205 or 210 kHz, respectively. Various defocus length ($f_d = 1.0\text{--}5.0$ mm), and power factor ($p = 30\% \text{--} 70\%$) were studied. The output laser power P is 20 W. The diameter of spot size ($D = 0.0535\text{--}0.1087$ mm) of the laser was directly measured under Long-depth-field Microscope (LDFM, Leica

IC90 E). The power density, ρ , is evaluated by [54]

$$\rho = 4Pp/\pi D^2 \quad (1)$$

The total interaction time between laser beam and MGs, t , is estimated by

$$t = Df\tau/v \quad (2)$$

Room-temperature uniaxial tensile tests were performed by a deformation device system (Kammrath Weiss GmbH DDS-3) at a strain rate of $1 \times 10^{-4} \text{ s}^{-1}$. Typical ribbon-length in tension was 28 mm where the welding joint was placed right in the middle. The amorphicity was checked by a lab X-ray diffractor (XRD, Bruker D8A A25) using Cu-K α radiation (wavelength of 1.5418 \AA), and reassured by synchrotron x-ray scattering measured at station 11-ID-C of the Advanced Photon Source, Argonne National Laboratory, using a 105.7 keV X-ray with a beam size of $500 \mu\text{m} \times 500 \mu\text{m}$ in transmission geometry at ambient conditions. Welded ribbons, with a typical thickness of 50–100 μm at the welding joint, are examined. Long-depth-field Microscope (LDFM, Leica IC90 E) was used to check the macro-morphology and SEM was applied to study the welding joints.

3. Results and discussion

By ns-pulsed laser welding, the MG ribbons were successfully welded into different shapes. For example, the $\text{Fe}_{78}\text{Si}_9\text{B}_{13}$ MG ribbons were welded into a bracelet and a “Möbius band” [Fig. 1(b)]; the welded bracelets can have different diameters [Fig. 1(c)]. Similar to that of the crystalline materials, the welding joints of the MGs consist of two parts, i.e. the fusion zone (FZ) and the heat-affected zone (HAZ) [Fig. 1(d)]. The size of FZ and HAZ are measured from both sides of the ribbon welding-joint. Fig. 1(e) schematically presents the welding joint from the side view, where the upside and downside are marked by U and D, respectively. Because the ribbons are very thin, the boundaries of both FZ and HAZ in side view are assumed straight.

After welding, the structural state of the welding joint was characterized by X-ray. The FZs and HAZs of the whole welding joints, on both U and D sides and along the welding direction, are all characterized, where only amorphous halos are detected, suggesting that the materials are not crystallized after welding [Fig. 2(a)]. In fact, fast determination of the maximum t can be performed by high-throughput laser scanning. Because t is altered by v , f and τ [Eq. (2)], a series of lines, corresponding to different t s, are first laser welded on the same MG ribbon and then checked under lab X-ray diffraction. Fig. 2(b) presents the structural check of the Ce-, La-, Zr-, Fe-based MGs at ρ of $2.0\text{--}5.1 \times 10^5 \text{ W mm}^{-2}$ where the maximum t to maintain amorphicity can be easily obtained from the amorphous/crystalline boundary. For example, at $\rho = 3.0 \pm 1.0 \times 10^5 \text{ W mm}^{-2}$, the maximum t to maintain amorphicity for the Ce-, La-, Zr-, Fe-based MGs, as presented in the inset of Fig. 2(b), are 0.20, 0.25, 0.26, 0.38 μs , respectively.

The effect of the defocus length (f_d) is tested by lap welding the $\text{Ce}_{65}\text{Al}_{10}\text{Cu}_{20}\text{Co}_5$ MG ribbons at a constant p of 70%. Fig. 3(a) exhibits the side, top and bottom views of the welding joints at f_d of 1.0, 2.5 and 5.0 mm, respectively. At f_d of 1.0 mm, welding fails as the welding joint breaks because of the excessive heating. At f_d of 2.5 mm, the FZ is a symmetric trapezoid where the U-FZ is slightly larger than the D-FZ. At f_d of 5.0 mm, the FZ trapezoid has a U-FZ much larger than its D-FZ. On the other hand, the U-HAZ almost equals the D-HAZ at f_d of 2.5 mm, but the U-HAZ is smaller than the D-HAZ at f_d of 5.0 mm [Fig. 3(b)]. The typical sizes of the FZ and HAZ at f_d of 2.5 mm are $260 \pm 10 \mu\text{m}$ and $190 \pm 10 \mu\text{m}$, respectively. For the mechanical property, the fracture strength (σ) can be as high as 70% of that of the parent MG at $f_d = 2.5\text{--}4$ mm [Fig. 3(c)]. In contrast, when f_d is smaller than 2.5 mm or larger than 4 mm, the fracture strength is reduced. Taking $f_d = 2.5\text{--}4$ mm as the optimal condition for laser welding, the corresponding power density (ρ), calculated from Eq. (1), is at $1\text{--}4 \text{ kW/mm}^2$.

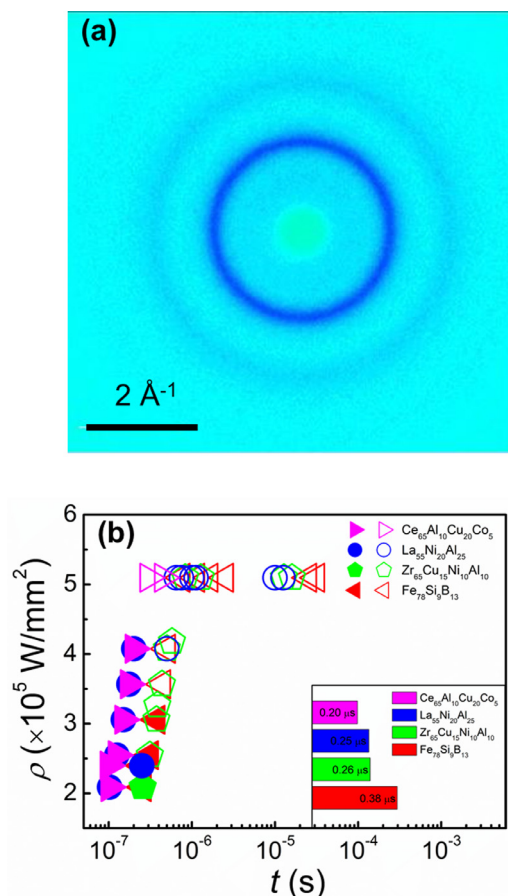


Fig. 2. The welding joints are kept amorphous after ns-pulsed laser welding. (a) Synchrotron X-ray scattering of the welding joint of the Ce-based MG ribbon. (b) The critical crystallization time can be quickly determined by varying the interaction time, t , in laser welding. The filled and open symbols represent amorphous and crystalline states.

The influence of the power factor (p) is tested during butt welding process of the $\text{Ce}_{65}\text{Al}_{10}\text{Cu}_{20}\text{Co}_5$ MG ribbons, where the f_d is fixed at 2.5 mm, corresponding to a D of 0.0684 mm. At $p = 30\%$, only FZ yet no obvious HAZ can be detected [Fig. 3(d)]. At $p = 50\%$ and 68%, the profiles of the welding joints [Fig. 3(e)] appear similar to that of $f_d = 2.5$ mm [Fig. 3(a)], and the HAZ to FZ ratios are in the range of 40%–70%. Meanwhile, there is also a p -dependence of the σ , and the maximum σ can be as high as 90% of that of the as-cast at $p = 50\%$ [Fig. 3(f)]. Taking $p = 40\%$ –50% as the optimal condition for welding, the corresponding ρ , calculated by Eq. (1), is at 0.7–1.6 kW/mm².

The present paper points out that the interaction time and the power density are the two main factors that influence the quality of the welding MG ribbons. Because most of the good glass formers of MGs will start crystallization in milliseconds at the crystallization temperatures [3], it is important and necessary to use *ms*- or *ns*-pulsed lasers for welding. By adjusting the v , f and τ , t can be controlled [Eq. (2)] within the “safe range” in the sense that crystallization can be avoided. It is then important to control the ρ of the laser to generate a nice profile of the welding joint so that the strength of the material can be maintained as much as possible.

The profile of the welding joint can be considered as the first evaluation of welding quality because the profile is closely linked to the fracture strength (Fig. 3). From our observation, a good profile should be a symmetric trapezoid with its U-FZ close to its D-FZ and a HAZ/FZ ratio within the range of 40%–70%. In contrast, bad profiles with either U-FZ much larger than D-FZ or the HAZ/FZ ratio is out of the range of 40%–70% are related to weaker joining. Because one can easily

measure the profiles of the welding joints under an optical microscope, the simple geometrical “criterion” can be used for primary estimation.

The success of welding is also connected to the proper selection of power density (ρ). The ρ is adjusted by either D or p [Eq. (1)]. When ρ is low, the ribbons are not welded through; when ρ is high, the ribbons are welded too much, reaching a condition called excessive penetration. In both cases, welding leads to low tensile strength. The fracture strength reaches a maximum at the optimal ρ . However, there is an apparent difference in the optimal condition between the lap and butt welding. This is because the sample thicknesses (h s) are different for lap and butt welding: h doubles in lap welding because two ends of the ribbons are lapped. It is then important to use ρ/h rather than ρ itself to select the optimal ρ for MG ribbon welding. For lap welding, ρ/h is 12–51 kW/mm³; for butt welding, ρ/h is 11–26 kW/mm³. Results show that the optimal ρ/h for MG welding agree well for lap and butt welding.

Fig. 4 summarizes the ρ/h and t of MG ribbon- and plate- welding. It is clear that welding succeeds when ρ/h is at the order magnitude of 10^4 – 10^5 W/mm³ as confirmed by both of our tests and literature. Note the optimal ρ/h is not limited to sample thickness, it works for both μm or mm thick MG specimen and might also be valid for MG of other h s like 100 nm MG thin films. Furthermore, if it is necessary to avoid crystallization, the *ms*-pulsed laser may only work for those MGs that are best glass formers, whereas *ns*-pulsed laser can be applied for more MGs with good glass-forming ability. As can be seen from Fig. 4, the total interaction time of the applied *ns*-pulsed laser is orders magnitude shorter than the boundary between the amorphous and the crystallized, leaving sufficient time for welding. The *ns*-pulsed laser then outweighs the *ms*-pulsed laser.

4. Conclusions

In summary, the present study demonstrates that metallic glass ribbons can be easily welded by nanosecond-pulsed laser. Through laser welding, origami or curvatures made by the MG thin ribbons can be preserved. The results also prove that *ns*-pulsed laser can weld MG ribbons in the air without crystallization, and the critical crystallization time can be quickly determined in a high-throughput way. The mechanical strength can be kept up to 70%–90% of the as-prepared ribbons at the optimal conditions of the defocus length and power factor. A welding processing map has been established which suggests that the optimal laser power-density per sample thickness is at the 10^4 – 10^5 W/mm³.

See supplementary material for the complete welding parameters (Table S1).

CRedit authorship contribution statement

Jin Feng Li: Conceptualization, Methodology, Formal analysis, Writing - review & editing. **Yong Hao Sun:** Conceptualization, Supervision, Writing - review & editing. **Da Wei Ding:** Methodology. **Wei Hua Wang:** Writing - review & editing. **Hai Yang Bai:** Conceptualization, Supervision, Writing - review & editing.

Declaration of Competing Interest

The authors declare no conflict of interests.

Acknowledgments

Prof. S. Lan from Nanjing University of Science and Technology and Prof. X. L. Wang from the City University of Hong Kong are acknowledged for their assistance in synchrotron X-ray scattering measurements. We are indebted to B.S. Dong and S.X. Zhou in the Advanced Technology and Materials Co., Ltd., of Central Iron and Steel Research Institute for supplying commercial samples. This research was supported by the Strategic Priority Research Program of the Chinese

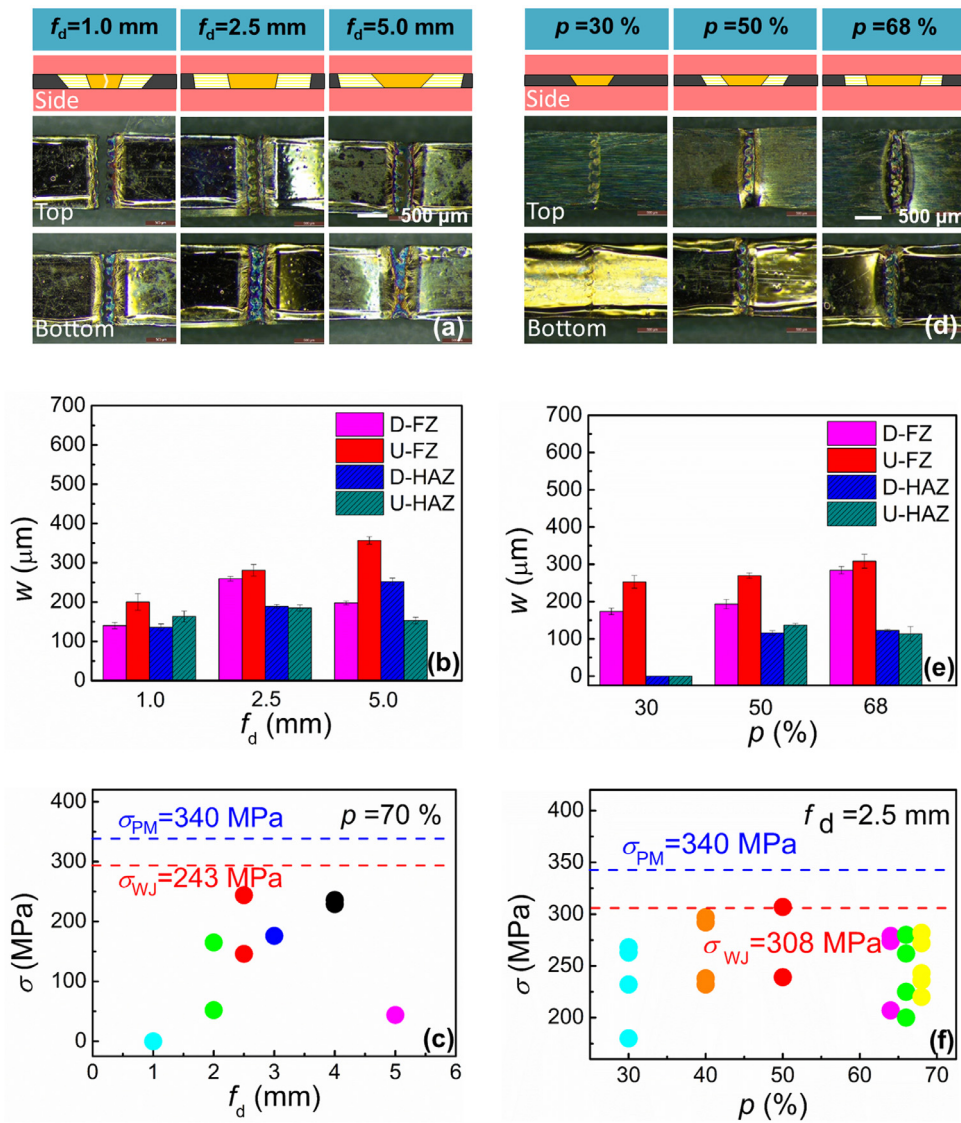


Fig. 3. Lap welding at $p = 70\%$ with $f_d = 1.0\text{--}5.0$ mm, and butt welding at $f_d = 2.5$ mm with $p = 30\%\text{--}68\%$. (a) The welding-joint topography from side, top and bottom views at f_{ds} . (b) The sizes of the U-FZ, D-FZ, U-HAZ, D-HAZ at f_{ds} . (c) The fracture strength of the welding joints (WJ) at f_{ds} . (d) The welding-joint topography from side, top and bottom views at p_s . (e) The sizes of the U-FZ, D-FZ, U-HAZ, D-HAZ at p_s . (f) The fracture strength of the welding joints (WJ) at p_s .

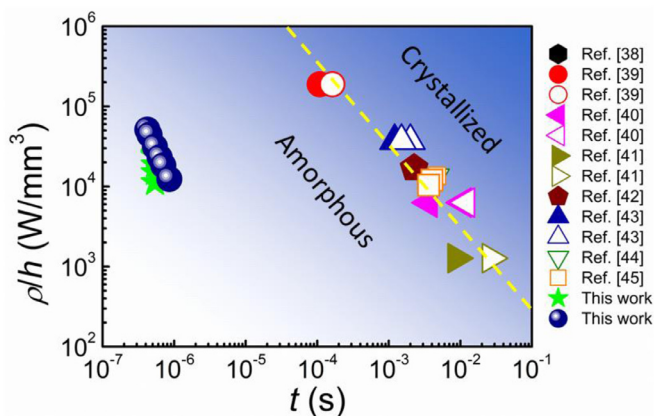


Fig. 4. The processing map of MG laser-welding. The power density per sample thickness (ρ/h) and the total interaction time (t) are critical for laser welding. (Solid markers: amorphous; open markers: crystallized).

Academy of Sciences (XDB30000000), National Key Research and Development Plan (2018YFA0703603), National Natural Science Foundation of China (11790291, 61999102, 61888102, 51871234 and 51971238) and Natural Science Foundation of Guangdong Province (2019B030302010).

Supplementary materials

Supplementary material associated with this article can be found, in the online version, at [doi:10.1016/j.jnoncrysol.2020.120016](https://doi.org/10.1016/j.jnoncrysol.2020.120016).

Reference

- [1] A. Inoue, Stabilization of metallic supercooled liquid and bulk amorphous alloys, *Acta Mater.* 48 (2000) 279–306.
- [2] C.C. Hays, J. Schroers, W.L. Johnson, T.J. Rathz, R.W. Hyers, J.R. Rogers, M.B. Robinson, Vitrification and determination of the crystallization time scales of the bulk-metallic-glass-forming liquid $Zr_{58.5}Nb_{2.8}Cu_{15.6}Ni_{12.8}Al_{10.3}$, *Appl. Phys. Lett.* 79 (2001) 1605–1607.
- [3] J.F. Löffler, Bulk metallic glasses, *Intermetallics* 11 (2003) 529–540.
- [4] W.H. Wang, C. Dong, C.H. Shek, Bulk metallic glasses, *Mater. Sci. Eng. R* 44 (2004) 45–89.
- [5] B. Zhao, B. Yang, A.S. Abyzov, J.W.P. Schmelzer, J. Rodriguez-Viejo, Q. Zhao,

- C. Schick, Y. Gao, Beating homogeneous nucleation and tuning atomic ordering in glass-forming metals by nanocalorimetry, *Nano Lett.* 17 (2017) 7751–7760.
- [6] Y. Kawamura, Y. Ohno, Metallurgical bonding of bulk metallic glasses, *Mater. Trans.* 42 (2001) 717–719.
- [7] Y. Kawamura, Y. Ohno, Superplastic bonding of bulk metallic glasses using friction, *Scr. Mater.* 45 (2001) 279–285.
- [8] H.S. Shin, Y.J. Jeong, H.Y. Choi, H. Kato, A. Inoue, Friction welding of $Zr_{55}Al_{10}Ni_5Cu_{30}$ bulk metallic glasses, *Mater. Trans.* 46 (2005) 2768–2772.
- [9] T. Shoji, Y. Kawamura, Y. Ohno, Joining of $Zr_{41}Be_{23}Ti_{14}Cu_{12}Ni_{10}$ bulk metallic glasses by a friction welding method, *Mater. Trans.* 44 (2003) 1809–1816.
- [10] Y. Kawamura, T. Shoji, Y. Ohno, Welding technologies of bulk metallic glasses, *J. Non-Cryst. Solids* 317 (2003) 152–157.
- [11] D. Makhanlall, G. Wang, J. Shen, Thermodynamic optimum friction welding of glassy rods, *J. Mater. Process. Technol.* 213 (2013) 1635–1639.
- [12] H.S. Shin, Y.J. Jeong, H.Y. Choi, H. Kato, A. Inoue, Joining of Zr-based bulk metallic glasses using the friction welding method, *J. Alloys Compd.* 434–435 (2007) 102–105.
- [13] G. Wang, Y.J. Huang, D. Makhanlall, J. Shen, Friction joining of $Ti_{40}Zr_{25}Ni_3Cu_{12}Be_{20}$ bulk metallic glass, *Mater. Process. Technol.* 212 (2012) 1850–1855.
- [14] C.H. Wong, C.H. Shek, Friction welding of $Zr_{41}Ti_{14}Cu_{12.5}Ni_{10}Be_{22.5}$ bulk metallic glass, *Scr. Mater.* 49 (2003) 393–397.
- [15] Y.S. Ji, H. Fujii, Y.F. Sun, M. Maeda, K. Nakata, H. Kimura, A. Inoue, K. Nogi, Friction stir welding of $Zr_{55}Cu_{30}Ni_5Al_{10}$ bulk metallic glass, *Mater. Trans.* 50 (2009) 1300–1303.
- [16] F.P. Li, D.C. Zhang, Z.C. Luo, C.G. Tan, J.G. Lin, Microstructure and mechanical properties of friction stir welded joint of $Zr_{46}Cu_{46}Al_8$ bulk metallic glass with pure aluminum, *Mater. Sci. Eng. A* 588 (2013) 196–200.
- [17] H.S. Shin, Y.C. Jung, Characteristics of dissimilar friction stir spot welding of bulk metallic glass to lightweight crystalline metals, *Intermetallics* 18 (2010) 2000–2004.
- [18] H.S. Shin, Y.-C. Jung, Characteristics of friction stir spot welding of Zr-based bulk metallic glass sheets, *J. Alloys Compd.* 504 (2010) S279–S282.
- [19] Y.F. Sun, Y.S. Ji, H. Fujii, K. Nakata, K. Nogi, Microstructure and mechanical properties of friction stir welded joint of $Zr_{55}Cu_{30}Al_{10}Ni_5$ bulk metallic glass with pure copper, *Mater. Sci. Eng. A* 527 (2010) 3427–3432.
- [20] Y.F. Sun, H. Fujii, Microstructure and mechanical properties of dissimilar spot friction stir welded $Zr_{55}Cu_{30}Al_{10}Ni_5$ bulk metallic glass to pure copper, *Intermetallics* 33 (2013) 113–119.
- [21] D. Wang, B.L. Xiao, Z.Y. Ma, H.F. Zhang, Friction stir welding of $Zr_{55}Cu_{30}Al_{10}Ni_5$ bulk metallic glass to Al–Zn–Mg–Cu alloy, *Scr. Mater.* 60 (2009) 112–115.
- [22] Y. Kawamura, Y. Ohno, Spark welding of $Zr_{55}Al_{10}Ni_5Cu_{30}$ bulk metallic glasses, *Scr. Mater.* 45 (2001) 127–132.
- [23] H. Kreye, M. Hammerschmidt, G. Reiners, Ultrasonic welding of metallic alloy glass to copper, *Scr. Mater.* 12 (1978) 1059–1061.
- [24] J. Kim, Weldability of $Cu_{54}Zr_{22}Ti_{18}Ni_6$ bulk metallic glass by ultrasonic welding processing, *Mater. Lett.* 130 (2014) 160–163.
- [25] M. Maeda, Y. Takahashi, M. Fukhara, X. Wang, A. Inoue, Ultrasonic bonding of $Zr_{55}Cu_{30}Ni_5Al_{10}$ metallic glass, *Mater. Sci. Eng. B* 148 (2008) 141–144.
- [26] H.L. Luo, N. Luo, X.J. Li, X. Sun, T. Shen, Z. Ma, Joining of $Zr_{60}Ti_{17}Cu_{12}Ni_{11}$ bulk metallic glass and aluminum 1060 by underwater explosive welding method, *J. Manu. Proc.* 45 (2019) 115–122.
- [27] M.Q. Jiang, B.M. Huang, C. Lu, L.H. Dai, Joining of bulk metallic glass to brass by thick-walled cylinder explosion, *Scr. Mater.* 97 (2015) 17–20.
- [28] Y. Kawamura, Liquid phase and supercooled liquid phase welding of bulk metallic glasses, *Mater. Sci. Eng. A* 375–377 (2004) 112–119.
- [29] Y. Kawamura, Y. Ohno, Successful electron-beam welding of bulk metallic glass, *Mater. Trans.* 42 (2001) 2476–2478.
- [30] Y. Kawamura, S. Kagao, Y. Ohno, Electron beam welding of Zr-based bulk metallic glass to crystalline Zr metal, *Mater. Trans.* 42 (2001) 2649–2651.
- [31] S. Kagao, Y. Kawamura, Y. Ohno, Electron-beam welding of Zr-based bulk metallic glasses, *Mater. Sci. Eng. A* 375–377 (2004) 312–316.
- [32] J. Kim, Y. Kawamura, Electron beam welding of the dissimilar Zr-based bulk metallic glass and Ti metal, *Scr. Mater.* 56 (2007) 709–712.
- [33] J. Kim, Y. Kawamura, Electron beam welding of Zr-based BMG/Ni joints: effect of beam irradiation position on mechanical and microstructural properties, *J. Mater. Process. Technol.* 207 (2008) 112–117.
- [34] J. Kim, Y. Kawamura, Dissimilar welding of $Zr_{41}Be_{23}Ti_{14}Cu_{12}Ni_{10}$ bulk metallic glass and stainless steel, *Scr. Mater.* 65 (2011) 1033–1036.
- [35] N.H. Tariq, M. Shakil, B.A. Hkhter, J.I. Akhter, M.A. Haq, N.A. Awan, Electron beam brazing of $Zr_{62}Al_{13}Ni_7Cu_{18}$ bulk metallic glass with Ti metal, *Vacuum* 101 (2014) 98–101.
- [36] G. Wang, Y.J. Huang, W. Cao, Z.J. Huang, M. Huttula, Y.S. Su, Caiwang Tan, Microstructure and crystallization mechanism of Ti-based bulk metallic glass by electron beam welding, *J. Manu. Proc.* 32 (2018) 93–99.
- [37] M. Watanabe, S. Kumai, G. Hagimoto, Q.S. Zhang, K. Nakayama, Interfacial microstructure of aluminum/metallic glass lap joints fabricated by magnetic pulse welding, *Mater. Trans.* 50 (2009) 1279–1285.
- [38] T.L. Shi, B. Chen, M. Li, F. Yan, G.L. Liao, Laser welding of annealed $Zr_{55}Cu_{30}Ni_5Al_{10}$ bulk metallic glass, *Intermetallics* 46 (2014) 111–117.
- [39] Y. Kawahito, T. Terajima, H. Kimura, T. Kuroda, K. Nakata, S. Katayama, A. Inoue, High-power fiber laser welding and its application to metallic glass $Zr_{55}Al_{10}Ni_5Cu_{30}$, *Mater. Sci. Eng. B* 148 (2008) 105–109.
- [40] J. Kim, D. Lee, S. Shin, C. Lee, Phase evolution in $Cu_{54}Ni_6Zr_{22}Ti_{18}$ bulk metallic glass Nd:YAG laser weld, *Mater. Sci. Eng. A* 434 (2006) 194–201.
- [41] J.H. Kim, C. Lee, J.H. Sun, S.Y. Shin, J.C. Bae, Pulsed Nd:YAG laser welding of $Cu_{54}Ni_6Zr_{22}Ti_{18}$ bulk metallic glass, *Mater. Sci. Eng. A* 449–451 (2007) 872–875.
- [42] B. Li, Z.Y. Li, J.G. Xiong, L. Xing, D. Wang, Y. Li, Laser welding of $Zr_{45}Cu_{48}Al_7$ bulk glassy alloy, *J. Alloys Compd.* 413 (2006) 118–121.
- [43] G. Wang, Y.J. Huang, M. Shagiev, J. Shen, Laser welding of $Ti_{40}Zr_{25}Ni_3Cu_{12}Be_{20}$ bulk metallic glass, *Mater. Sci. Eng. A* 541 (2012) 33–37.
- [44] H.S. Wang, H.G. Chen, H.G. Chen, J.S.C. Jang, M.S. Chiou, Combination of a Nd:YAG laser and a liquid cooling device to ($Zr_{53}Cu_{30}Ni_9Al_8$) $Si_{0.5}$ bulk metallic glass welding, *Mater. Sci. Eng. A* 528 (2010) 338–341.
- [45] H.S. Wang, H.G. Chen, J.S.C. Jang, Microstructure evolution in Nd:YAG laser-welded ($Zr_{53}Cu_{30}Ni_9Al_8$) $Si_{0.5}$ bulk metallic glass alloy, *J. Alloys Compd.* 495 (2010) 224–228.
- [46] H.S. Wang, M.S. Chiou, H.G. Chen, J.S.C. Jang, The effects of initial welding temperature and welding parameters on the crystallization behaviors of laser spot welded Zr-based bulk metallic glass, *Mater. Chem. Phys.* 129 (2011) 547–552.
- [47] H.S. Wang, M.S. Chiou, H.G. Chen, J.S.C. Jang, J.W. Gu, Microstructure evolution of the laser spot welded Ni-free Zr-based bulk metallic glass composites, *Intermetallics* 29 (2012) 92–98.
- [48] H.S. Wang, T.H. Lu, H.G. Chen, J.H. Pan, J.S.C. Jang, Microstructural evolution and properties of laser spot-welded Zr Al Co Ta bulk metallic glass under various initial welding temperatures, *Intermetallics* 108 (2019) 39–44.
- [49] H.S. Wang, Y.Z. Su, J.S.C. Jang, H.G. Chen, A comparison of crystallization behaviors of laser spot welded Zr–Cu–Ag–Al and Zr–Cu–Ni–Al bulk metallic glasses, *Mater. Chem. Phys.* 139 (2013) 215–219.
- [50] H.S. Wang, J.Y. Wu, Y.T. Liu, Effect of the volume fraction of the ex-situ reinforced Ta additions on the microstructure and properties of laser-welded Zr-based bulk metallic glass composites, *Intermetallics* 68 (2016) 87–94.
- [51] A. de Pablos-Martín, T. Hoche, Laser welding of glasses using a nanosecond pulsed Nd: YAG laser, *Opt. Lasers Eng.* 90 (2017) 1.
- [52] D. Faubert, S.L. Chin, Short laser pulse generation: part one, *Opt. Laser Technol.* 14 (1982) 197–206.
- [53] C. Kumar, N. Patel, Lasers-their development and applications at at&t bell laboratories, *IEEE J. Quantum Electron.* 20 (1984) 561–576.
- [54] J.D. Majumdar, I. Manna, Laser material processing, *Int. Mater. Rev.* 56 (2011) 341.